processes

MDPI

Article

Experimental Study on the Influence of Wind Speed on the Start-Up Characteristics and Thermoelectric Generation Characteristics of Gravity Heat Pipe in Gangue Dump

Bailin Zhang [1,2], Shuhua Fang [1,*], Songlin Zhang [2], Runxu Zhang [2] and Yu Zang [3]

[1] School of Electrical Engineering, Southeast University, Nanjing 210096, China
[2] College of Safety and Emergency Management Engineering, Taiyuan University of Technology, Taiyuan 030024, China
[3] School of Hydro Science and Engineering, Taiyuan University of Technology, Taiyuan 030024, China
* Correspondence: zy_tyut2022@163.com

Abstract: As an efficient heat exchange component, the gravity heat pipe can effectively control the accumulated temperature inside gangue dumps and enable reuse of transferred heat. This study establishes a similar simulation experimental platform for gravity heat pipes to control gangue dumps and thermoelectric generation. The influence of wind speed on the start-up performance and isothermal performance of gravity heat pipes is analyzed, along with the impact of wind speed on their thermoelectric generation performance. Initially, the optimal working fluid height and heating height are determined, followed by a comparison and analysis of the isothermal performance, start-up performance, and thermoelectric generation performance of the gravity heat pipe under different wind speeds. The results indicate that at a wind speed of 1.0 m/s, the gravity heat pipe exhibits better start-up and isothermal performance. At a wind speed of 2.0 m/s, the thermoelectric power generation reaches its peak. In the range of 1.0~2.0 m/s wind speeds, the curve of thermoelectric generation exhibits the most fluctuations.

Keywords: wind speed; start-up characteristic; thermoelectric generation; gravity heat pipe

Citation: Zhang, B.; Fang, S.; Zhang, S.; Zhang, R.; Zang, Y. Experimental Study on the Influence of Wind Speed on the Start-Up Characteristics and Thermoelectric Generation Characteristics of Gravity Heat Pipe in Gangue Dump. *Processes* **2023**, *11*, 2429. https://doi.org/10.3390/pr11082429

Received: 16 July 2023
Revised: 2 August 2023
Accepted: 6 August 2023
Published: 12 August 2023

1. Introduction

The gangue dump refers to the waste generated during coal mining [1]. Long-term accumulation of gangue can result in internal spontaneous combustion and an increase in the accumulated temperature. This, in turn, leads to a higher concentration of toxic and hazardous gases, such as nitrogen oxides and sulfur oxides, in the surrounding air, posing a serious threat to the ecological environment [2–4]. With its excellent isothermal performance, the gravity heat pipe (GHP) can rapidly transfer the deep-seated accumulated heat to the ground, effectively preventing an increase in the internal temperature of the gangue dump [5–7]. Therefore, the GHP can effectively control the environmental conditions within the gangue dump.

Heat pipes have been widely utilized as efficient heat conduction components in various applications, including ambient temperature [8], spacecraft thermal management [9], nuclear reactor system [10], solar energy [11], macro-scale thermal management [12], and cooling of electronics [13]. The previous literature has primarily focused on investigating heat pipe characteristics within specific application domains. In the context of GHPs, numerous researchers have conducted fundamental experimental studies. For instance, Mahdavi et al. [14] explored the impact of working fluid fill volume, inclination angle, and heat input on the equivalent thermal resistance of heat pipes. Their findings indicated a negligible effect of the inclination angle on the performance of gravity-assisted heat pipes, whereas, for gravity-opposed heat pipes, an increased inclination angle resulted in a higher thermal resistance due to an elevated temperature difference between the evaporator and

condenser. Zhang et al. [15] utilized Visual Basic programming simulation analysis to investigate influencing factors on the heat transfer performance of heat pipe heat exchangers, including tube length, diameter, tube spacing, and fin parameters. Xiong et al. [16] conducted a fundamental experimental study on the start-up characteristics of heat pipes, employing a dedicated molten–salt mixture as the working fluid. Eui Guk Jung et al. [17] proposed a bypass line to enhance the dry-out prevention performance during heat pipe operation. Notably, using a horizontal arrangement led to an approximately 35.5% increase in the maximum heat transfer rate. Naruka et al. [18] comprehensively examined cylindrical heat pipes and determined that the optimal inclination angle for efficient heat transfer was 45°. Moreover, heat pipes can exhibit unique properties in the presence of a magnetic field and wind field. The magnetic field can enhance the heat transfer coefficient, with a significant impact from the inclination angle [19,20]. Additionally, the wind field can promote working fluid circulation in heat pipes. Increased cooling wind speed leads to decreased start-up time and temperature for pulsating heat pipes, while stability improves [21,22]. These distinctive properties lay the foundation for the application of GHPs in controlling the environmental conditions within gangue dumps.

Due to the unique thermal conditions within gangue dumps, the design of a specialized GHP for these dumps differs from heat pipes used in other fields. Upon completion of the gangue dump formation, a thin topsoil layer is applied to minimize oxygen contact with the internal gangue [23]. Given the substantial amount of heat energy present in the gangue dump, the GHP efficiently transmits this heat to the ground. Figure 1 illustrates an experimental site in Shanxi, China, where the GHP is implemented. During the process of controlling the cumulative temperature of the gangue dump, the working fluid contained within the GHP absorbs the heat from the gangue dump and undergoes vaporization. The resulting gas ascends to the condensation section of the GHP, where it liquefies and releases heat. Simultaneously, the released heat enables a thermoelectric generator to produce electricity, thus achieving the dual objectives of regulating the cumulative temperature of the gangue dump and generating electricity.

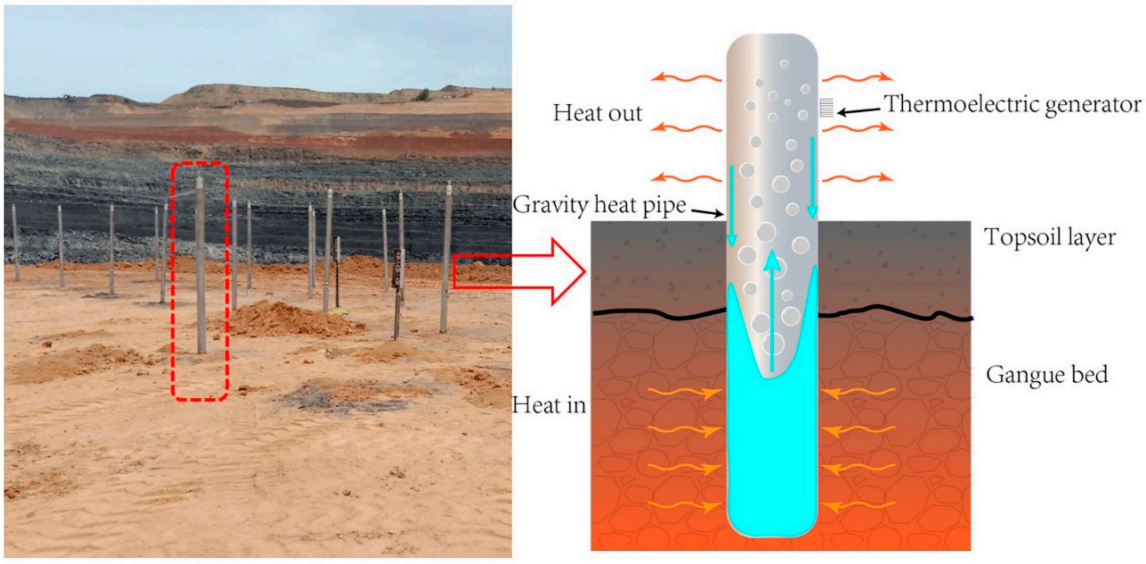

Figure 1. Experimental site of GHP in waste rock dump and heat transfer diagram of GHP.

2. Experiment Setup

The characteristics of heat pipes have been extensively investigated by numerous researchers using similar physical experimental setups [24–27]. In order to examine the optimal parameter matching for the gravity heat pipe (GHP) and explore the thermoelectric generation properties of the condensation section of the GHP, this study employs a similar simulation experiment approach. A scaled-down experimental model of a heat

pipe, representing the GHP used in gangue dumps, was fabricated. The corresponding experimental platform was constructed in the laboratory, as depicted in Figure 2. The installation principles of GHP sensors, indicating the sensor placement locations and the definitions of various parameters, are illustrated in Figure 3.

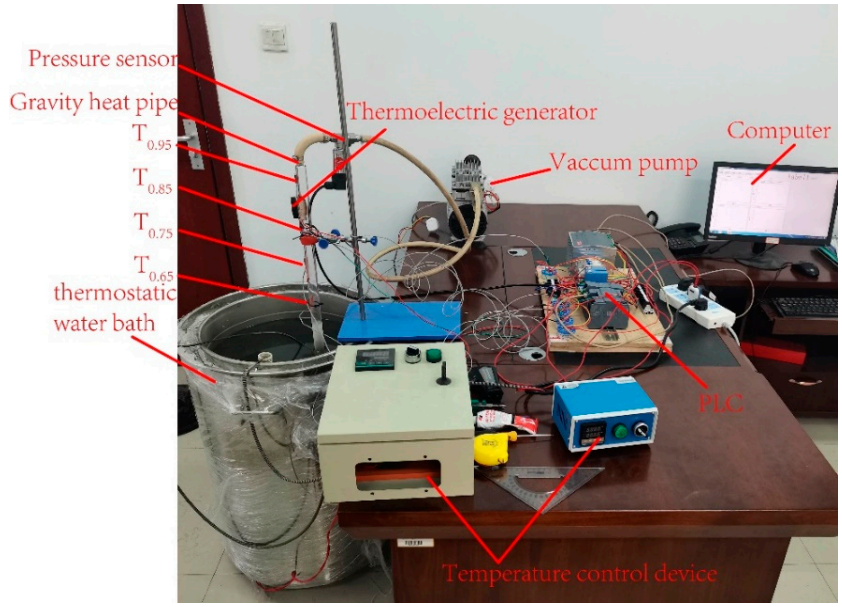

Figure 2. GHP experimental device.

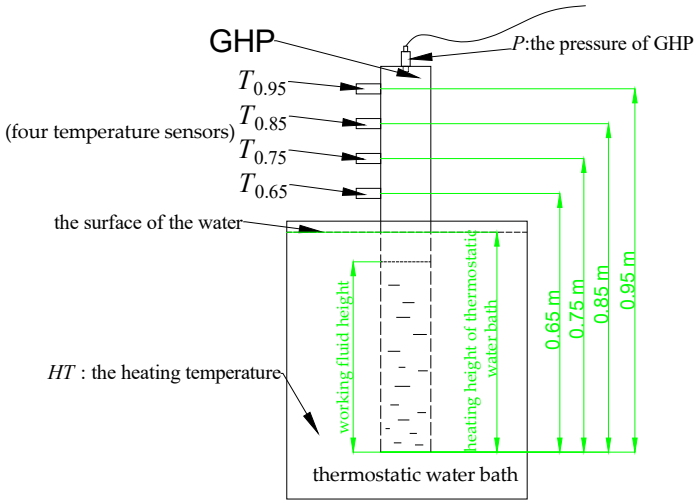

Figure 3. Schematic diagram of experimental device sensor installation.

The experimental setup consists of a thermostatic water bath, four temperature sensors, a GHP, a pressure sensor, a thermoelectric generator, a temperature control device, a programmable logic controller (PLC), a vacuum pump, and a computer system. The temperature control device regulates the heating temperature of the thermostatic water bath. The evaporation section of the GHP is immersed in the thermostatic water bath. Temperature sensors are strategically positioned at 0.65, 0.75, 0.85, and 0.95 m along the condensation section. The thermoelectric generator is installed at the 0.9 m position.

The computer system, integrated with the PLC, continuously monitors the internal pressure of the GHP, as well as the current, voltage, and real-time temperatures at each measuring point. Prior to conducting the experiment, a specified amount of working fluid is loaded into the GHP, and the gas within the system is evacuated to a fixed pressure

using a vacuum pump. The valve between the vacuum pump and the pressure sensor is manually closed to ensure no air leakage occurs within the GHP.

Figure 4 provides an overview of the experiment, which initially investigates the influence of heating height to determine the optimal heating height for the GHP. Subsequently, the impact of working fluid height on the GHP is examined to identify the optimal working fluid height. Variations in wind speed are then explored to observe their effects on the GHP. Finally, individual experiments are conducted to assess the start-up performance and temperature difference in the power generation capabilities of the GHP under different wind speeds. Table 1 summarizes the relevant parameters of the experimental setup.

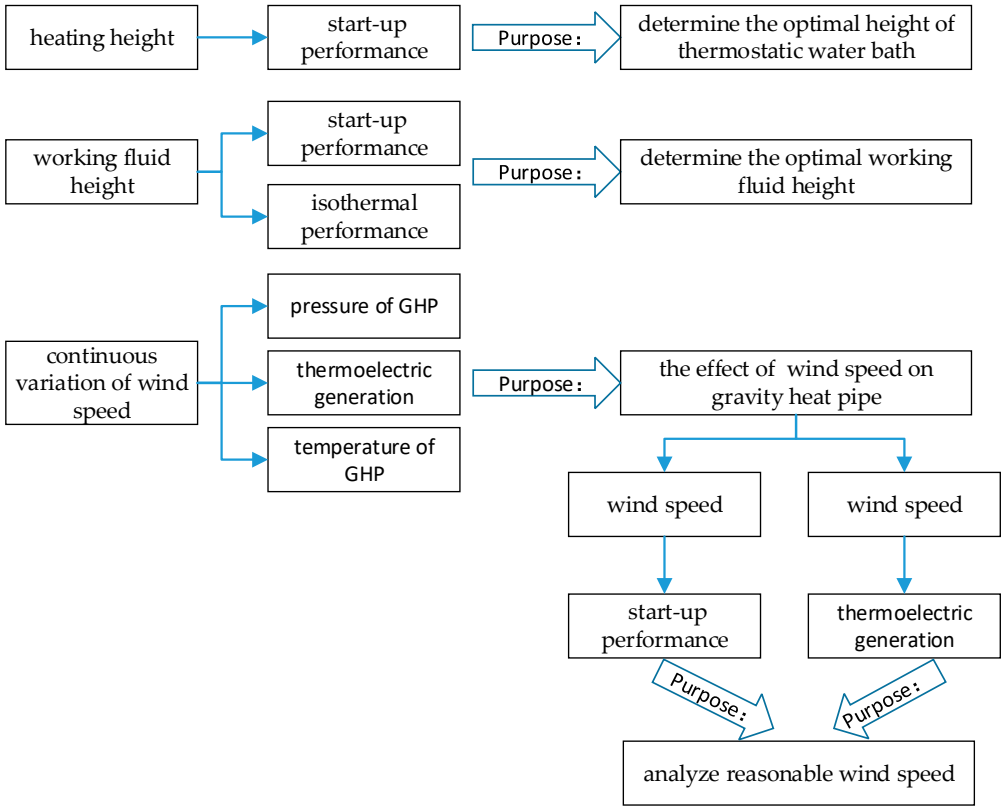

Figure 4. Experimental scheme of GHP.

Table 1. Summary table of relevant parameters of the experimental device.

Properties	Parameter Description
Total length of the GHP	1000 mm
Installation position of temperature sensor	0.65, 0.75, 0.85, 0.95 m
Installation position of thermoelectric generator	0.9 m
Working fluid	water
Thermostatic water bath heating power	4 kW
Minimum pressure of vacuum pump	0.002 MPa

3. Results and Discussion

3.1. Effect of Heating Height of Thermostatic Water Bath on Start-Up Performance of GHP

The influence of heating height on the start-up characteristics of the GHP was investigated through comparative experiments, as illustrated in Figure 5. The experimental parameters were set as follows: the heating temperature ranged from 0 to 100 °C, the initial absolute pressure was 0.002 MPa, the working fluid height was 200 mm, and the wind speed was 0 m/s. The start-up characteristics of the heat pipe were examined at constant temperature water bath heating heights of 250 mm, 400 mm, and 600 mm.

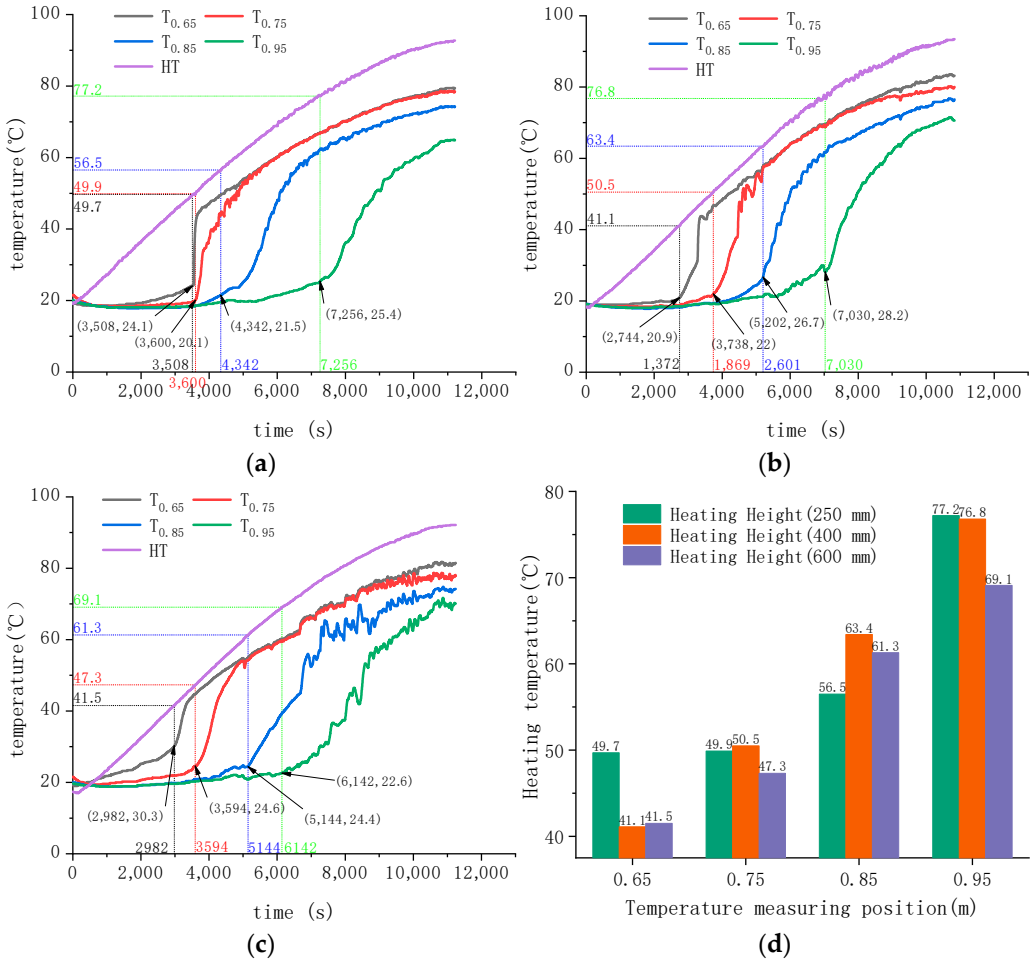

Figure 5. Curve of influence of different thermostatic water bath heating heights on start-up of GHP. (wind speed is 0 m/s). (**a**) The heating height of thermostatic water bath is 250 mm. (**b**) The heating height of thermostatic water bath is 400 mm. (**c**) The heating height of thermostatic water bath is 600 mm. (**d**) The influence of the change of heating height of thermostatic water bath on the initial start-up temperature of each temperature measuring point of GHP.

Figure 5a illustrates the temperature profiles of individual temperature sensors at a heating height of 250 mm. The observations reveal that during the initial stage of continuous heating, there was no significant variation in the temperature of the GHP's condenser region. However, when the heating temperature reached 49.7 °C, the temperature at 0.65 m experienced a rapid increase from 25 °C to 45 °C within a short time duration. Subsequently, after 92 s, a noticeable rise in temperature was observed at 0.75 m, and after 742 s, the GHP ascended to 0.85 m. At a heating temperature of 77.2 °C, the GHP was fully activated, extending up to 0.95 m.

Figure 5b presents the temperature profiles of each temperature sensor at a heating height of 400 mm. It is evident that as the heating temperature increases, the GHP initiates operation at 0.65 m when the heating temperature reaches 41.1 °C and at 0.75 m when the heating temperature rises to 50.5 °C. Notably, the initial temperatures at these two points exhibit a vibration phenomenon. Subsequently, when the heating temperature of the heat pipe reaches 63.4 °C, the GHP commences operation up to 0.85 m and attains complete activation when the temperature reaches 76.8 °C.

Figure 5c illustrates the temperature curves at each point for a heating height of 600 mm. It can be observed that at a heating temperature of 41.5 °C, initiation occurs at 0.65 m; at 47.3 °C, initiation takes place at 0.75 m; at 61.3 °C, initiation is observed at 0.85 m; and, finally, at 69.1 °C, the heating commences at 0.95 m.

In Figure 5d, the histogram showcases the start-up temperatures for each position at different heating heights. It is noticeable that the initial start-up temperature of the heat pipe with a heating height of 600 mm is 16.5% lower than that with a heating height of 250 mm. However, it is nearly the same as the start-up temperature of the heat pipe with a heating height of 400 mm. This similarity can be attributed to the increased heating height facilitating enhanced boiling and vaporization of the internal working fluid.

Based on the aforementioned figures, it is evident that the GHP achieves the shortest time for complete startup at a heating height of 600 mm. This occurs with a lowest heating temperature of 69.1 °C, which is 10.0% lower than the heating temperature at a heating height of 400 mm and 10.5% lower than the temperature at a heating depth of 250 mm. These research findings are consistent with references [28,29], indicating a regular pattern. Generally, the start-up temperatures of each point in the heat pipe with a heating height of 600 mm are relatively lower under these three conditions. This can be attributed to the increased contact area between the constant temperature water bath and the heat pipe, resulting from the increased heating height, facilitating enhanced heat transfer to the GHP. However, it is noteworthy that the increase in heating height does not linearly affect the start-up characteristics of the heat pipe, particularly at a heating height of 400 mm. For instance, when the heating height is 400 mm and 600 mm, the start-up temperature at 0.75 m in Figure 5b is higher than that in Figure 5a, and the start-up temperature at 0.85 m in Figure 5b,c is higher than that in Figure 5a. This phenomenon occurs due to the rapid increase in internal pressure of the heat pipe with temperature as the heating height increases, thereby suppressing the vaporization of the working fluid inside the heat pipe. Figure 5b,c also demonstrate larger temperature fluctuations in this section. However, the initial start-up temperature in Figure 5b,c is the lowest, and the final start-up temperature in Figure 5c is the lowest. The disparity among the final values of the temperature measurement point curves indicates that the temperature in Figure 5a is higher than that in Figure 5b, and the temperature in Figure 5b is higher than that in Figure 5c, suggesting that Figure 5c exhibits the best isothermal performance. Consequently, it can be concluded that the heat pipe demonstrates optimal start-up performance when the heating height is set to 600 mm.

3.2. Effect of Working Fluid Height Change on Start-Up Performance and Isothermal Performance of GHP

The start-up and isothermal performances of the GHP with different working fluid heights are illustrated in Figure 6. The heating temperature ranges from 0 to 100 °C, the initial absolute pressure is set at 0.002 MPa, the heating height is fixed at 600 mm, and the wind speed remains at 0 m/s. Notably, the working fluid height exerts a significant influence on both the start-up characteristics and isothermal behavior of each point in the GHP.

In Figure 6a, representing a working fluid height of 200 mm, it can be observed that the largest variance of the four temperature measuring points occurs when the heating temperature reaches 62 °C, reaching a value of 291. This indicates poor isothermal performance during this period. Subsequently, the variance exhibits minor fluctuations between 5132 s and 7162 s near its maximum value before gradually decreasing. When the heating temperature reaches 92 °C, the variance at each point becomes the smallest, measuring 48. This suggests that the GHP achieves a stable working state when the temperature exceeds 92 °C.

Turning to Figure 6b, which corresponds to a working fluid height of 300 mm, it is noteworthy that the largest variance in the four temperature measuring points occurs when the heating temperature rises to 74 °C, reaching 264. This signifies relatively poor isothermal performance at this stage. However, unlike in Figure 6a, the period with the worst isothermal performance in Figure 6b does not persist but rapidly diminishes as the temperature increases. When the heating temperature reaches 91 °C, the variance at each

temperature measuring point becomes the smallest, measuring 71. This suggests that the GHP attains a stable working state when the temperature surpasses 91 °C.

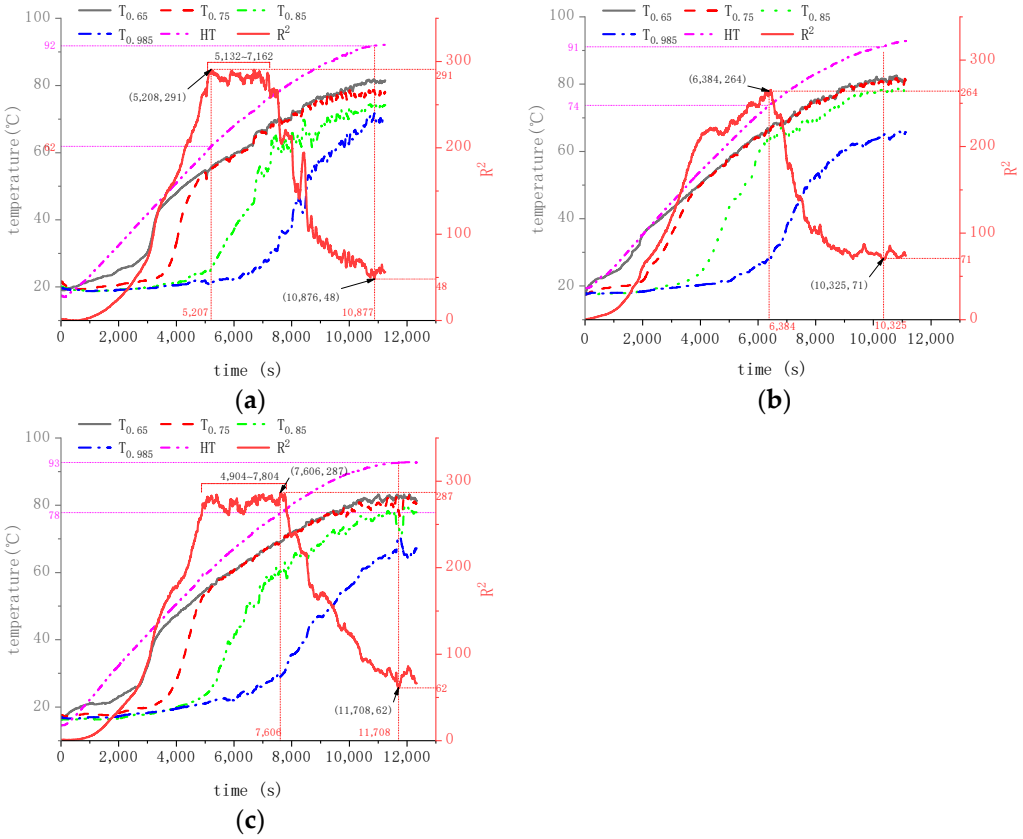

Figure 6. Temperature curve and variance curve of GHP under different working fluid heights. (R^2 represents the variances of $T_{0.65}$, $T_{0.75}$, $T_{0.85}$, and $T_{0.95}$. Wind speed is 0 m/s.) (**a**) The working fluid height variation of working fluid is 200 mm. (**b**) The working fluid height variation of working fluid is 300 mm. (**c**) The working fluid height variation of working fluid is 400 mm.

In Figure 6c, representing a working fluid height of 400 mm, the largest variance in the four temperature measuring points occurs when the heating temperature reaches 78 °C, reaching 287. This indicates that the isothermal performance is the poorest at this point. The variance exhibits minor fluctuations between 4904 s and 7804 s near its maximum value before gradually decreasing. When the heating temperature reaches 93 °C, the variance at each point becomes the smallest, measuring 62. This suggests that the GHP has reached a stable working state when the temperature exceeds 93 °C.

From Figure 6a–c, it can be observed that the worst point of isothermal performance for the GHP occurs between $T_{0.85}$ and $T_{0.95}$ during start-up. The analysis indicates that at this stage, $T_{0.65}$ and $T_{0.75}$ have already started and exhibit good isothermal performance. However, when $T_{0.85}$ and $T_{0.95}$ are started, the boiling of the internal working fluid needs to be further intensified. As the working fluid steam carrying a large amount of heat rises, the isothermal properties of $T_{0.65}$ and $T_{0.75}$ are compromised, leading to a rapid increase in the temperature of $T_{0.85}$ and $T_{0.95}$ and a decline in the isothermal performance of the GHP during this period.

The heating temperature corresponding to stable isothermal performance of the GHP is 92 °C in Figure 6a, 91 °C in Figure 6b, and 93 °C in Figure 6c. The difference between these three temperatures is not significant, indicating that the change in working fluid height has little effect on the start-up and ending temperature of the GHP. Based on the above analysis, increasing the working fluid height gradually raises the heating temperature corresponding

to the maximum temperature variance at each point, indicating that more heat is required for the increased working fluid.

In Figure 6b, the maximum variance of temperature at each point during start-up is the minimum, and the temperature curve does not exhibit continuity at this maximum variance. The temperature curves at the four points in Figure 6b show the smallest fluctuations, indicating that when the working fluid height is 300 mm and the filling rate is 50%, the GHP starts most smoothly and exhibits the best starting characteristics. This finding is consistent with reference [30], which suggests an optimal filling rate of 40%, and reference [31], which indicates that a filling rate of less than 50% is optimal. Thus, the optimal filling rate determined in this study is 50%.

3.3. Influence of Continuous Variation of Wind Speed on GHP

In order to investigate the influence of wind speed on the temperature of the GHP system, a thermostatic water bath is set at 100 °C to fully activate the GHP. It is essential that the wind direction faces the thermoelectric generator. As shown in Figure 7, when there is no wind, the evaporation section's temperature is 91 °C, and $T_{0.65}$, $T_{0.75}$, and $T_{0.85}$ are approximately 78 °C, indicating favorable isothermal characteristics. However, the temperature at 0.95 m is 64 °C, with a corresponding current and voltage of 0.01 A and 0.17 V, respectively. The internal pressure remains stable at 0.07 MPa. At this stage, the GHP is in a critical state of full start-up and is highly sensitive to wind speed.

When the wind speed increases to 0.3 m/s, there is no noticeable change in the stability of the heating section due to its position within the thermostatic water bath. However, the temperatures at 0.65 m, 0.75 m, and 0.85 m in the condensing section experience a brief decline followed by an increase, resulting in an overall temperature drop of 3.6%, with a decrease of 5.5% and subsequent rise of 1.9%. Conversely, the temperature at 0.95 m shows no significant increase following an initial drop of 8.6%. Throughout the process at 0.3 m/s, the temperature exhibits a slow and gradual decrease. Concurrently, there is a significant increase in both current and voltage values, followed by large fluctuations. The pressure inside the heat pipe remains relatively stable. This phenomenon occurs because the micro airflow carries away heat from the GHP, causing a delayed circulation of the internal working fluid due to the thermal resistance of the heat pipe. As a result, each point's temperature decreases under the airflow, causing an instantaneous increase in the temperature difference across the thermoelectric generator and consequently enhancing power generation. With the stabilization of the airflow, the working fluid circulation within the GHP is rebalanced. The temperatures at 0.65 m, 0.75 m, and 0.85 m increase, while the temperature at 0.95 m remains unchanged. This indicates that the highest point of condensation heat release from the internal working fluid gas has shifted downward, preventing some gases from rising to 0.95 m for condensation. Notably, the thermoelectric generator is installed at 0.9 m. Based on the fluctuation of the curve, it is evident that this location falls within the unstable condensation region, leading to temperature fluctuations and subsequently affecting thermoelectric power generation.

When the wind speed increases from 0.3 m/s to 0.5 m/s, there is a slight initial drop in temperature at each point, followed by a sudden rise that, eventually, stabilizes. This fluctuation becomes more pronounced from 0.65 m to 0.95 m. It indicates that as the wind speed further increases, the heat dissipation capacity of the condensation section of the GHP improves. The abrupt change in wind speed causes a short-term temperature fluctuation, which gradually stabilizes over time. Under the condition of 0.5 m/s, the temperature of the GHP decreases, with a significant decrease in the high areas and a slight decrease in the low areas. The current and voltage curves of the thermoelectric generator show a brief increase followed by a decline, eventually reaching a relatively stable state. The stability at the 0.5 m/s stage is better than at 0.3 m/s, indicating a downward shift of the unstable point of gas condensation.

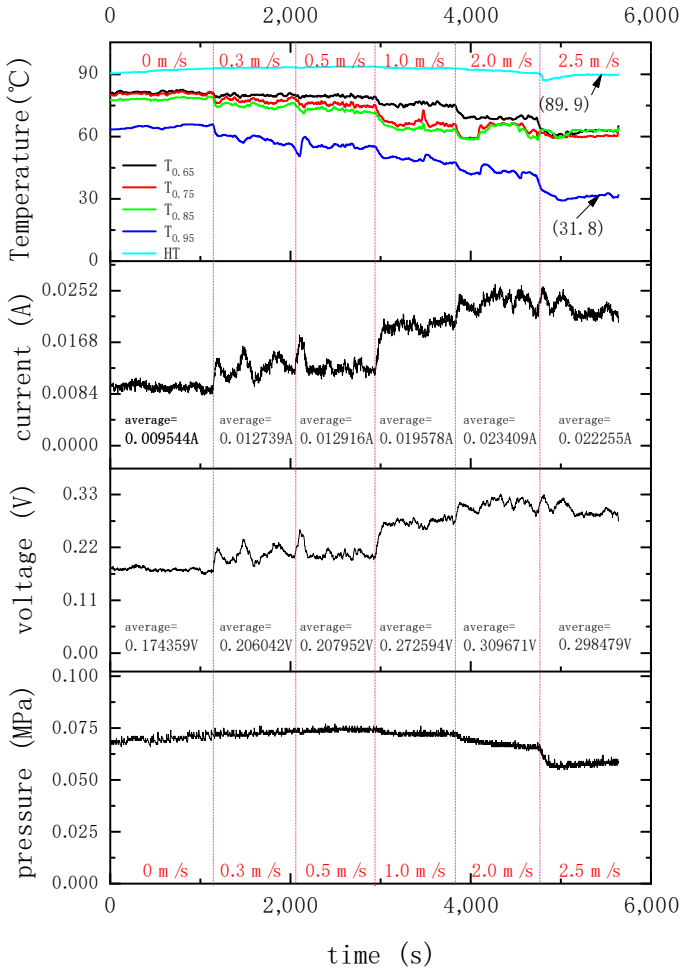

Figure 7. The impact of continuous changes in wind speed on temperature and thermoelectric generation, and internal pressure of each point of the GHP when the heating temperature is 100 °C, the initial absolute pressure is 0.002 MPa, the working fluid height is 300 mm, and the heating height is 600 mm.

As the wind speed increases from 0.5 m/s to 1.0 m/s, the temperature at each point decreases by approximately 8%, after which it stabilizes. The voltage and current show obvious increases during this period, with the current increasing by 51.6% and the voltage increasing by 31.1%. Further analysis reveals that the increased airflow accelerates the temperature cooling of the condensation section of the GHP. However, the heat in the evaporation section is insufficient to fully compensate for the heat loss, resulting in a temperature drop at each point. The amplitude of the temperature drop on the contact surface between the thermoelectric generator and the air is greater than that on the contact surface with the heat pipe, leading to an increase in temperature difference and, subsequently, power generation. The temperatures at 0.75 m, 0.85 m, and 0.95 m initially fluctuate and then stabilize after 3470 s. Considering the fluctuation amplitudes of temperature, current, and voltage, the inconsistency in their fluctuation patterns during the initial period of airflow adjustment can be observed. Moreover, the amplitude of current and voltage fluctuation is smaller than that of temperature, indicating the possible influence of unstable airflow in this phenomenon.

When the wind speed increases from 1.0 m/s to 2.0 m/s, there is a noticeable decrease in temperature at each point, accompanied by a further increase in current and voltage after a period of stabilization. Compared to 1.0 m/s, the current and voltage increase by 19.6% and 13.6%, respectively. During this stage, the fluctuations in voltage and current are more

pronounced than in the previous stage. Simultaneously, the internal pressure of the GHP experiences a significant decrease of 5.6%. This phenomenon occurs because the wind's heat dissipation capacity surpasses the heat input of the GHP's evaporation section at this stage. The temperature drop at 0.95 m is substantial, indicating a reduction in the amount of internal working fluid reaching that point. The slow increase in the current–voltage curve reflects a gradual rise in the thermoelectric generator's temperature difference.

As the wind speed increases from 2.0 m/s to 2.5 m/s, the temperature of the heating section experiences its first decrease, dropping to 89.9 °C, while the temperature at 0.95 m significantly reduces to 31.8 °C, resulting in a temperature difference of 58.1 °C. The temperatures at 0.65 m, 0.75 m, and 0.85 m also show significant decreases. These findings indicate that the GHP's isothermal performance begins to deteriorate, with reductions in both current and voltage compared to the previous stage. Furthermore, the internal pressure of the heat pipe decreases by 13.2%, suggesting a slowdown in the internal working fluid cycle due to the temperature drop. Overall, the GHP's performance starts to decline.

Based on the relationship between wind speed and temperature curve mentioned above, it aligns with references [21,32,33]. The analysis demonstrates that wind speed has a significant impact on the temperature, power generation, and internal pressure of the GHP. As the wind speed gradually increases from 0, the comprehensive performance of the GHP initially improves and then deteriorates. When the wind speed reaches 2 m/s, the thermoelectric generator achieves its maximum power generation. Compared to a wind speed of 0 m/s, the current generated by the thermoelectric generator is 145.3% higher, and the voltage is 77.6% higher. At this point, the pressure inside the heat pipe starts to slightly decrease, indicating that the GHP's performance is optimal when the wind speed is 2 m/s.

3.4. Influence of Wind Speed on Start-Up Performance of GHP

The heat dissipation performance of the GHP is greatly influenced by wind speed. In this study, we investigate the temperature variation at different points of the GHP under various wind speeds, ranging from 0 m/s to 2.5 m/s. The GHP has a heating temperature range of 0 to 100 °C, an initial absolute pressure of 0.002 MPa, a heating height of 600 mm, and a working fluid height of 300 mm.

Figure 8a illustrates the temperature variation at different points of the GHP when the wind speed is 0 m/s. As the temperature gradually increases, the evaporation section reaches 0.65 m at 43.1 °C, 0.75 m at 52.8 °C, 0.85 m at 63.5 °C, and 0.95 m at 77.6 °C.

Figure 8b shows that as the wind speed increases from 0 m/s to 0.3 m/s, the start-up temperature at each measuring point decreases. Specifically, the temperature at 0.65 m, 0.75 m, 0.85 m, and 0.95 m decreases to 31.0 °C, 41.9 °C, 56.5 °C, and 72.2 °C, respectively. This phenomenon indicates that the wind accelerates the heat dissipation in the condensation section of the GHP, thereby increasing the efficiency of the internal working fluid circulation. The temperature curves at 0.65 m, 0.75 m, and 0.85 m remain close to each other during the later stage of temperature measurement, indicating good isothermal performance within this range. However, the temperature curve at 0.95 m deviates from the other three curves. When this observation is combined with the analysis in the previous section, it suggests that the wind affects the position where gas condenses. Comparing the temperature curve at 0.95 m with that in Figure 8a, the temperature difference is small, indicating that the working fluid at 0.95 m has not decreased significantly. This further suggests that wind accelerates the internal working fluid circulation of the GHP.

Furthermore, in Figure 8, an abnormal fluctuation is observed in the temperature curve at 0.85 m at 6548 s, as well as some minor fluctuations at 0.65 m and 0.75 m. This occurs during the start-up phase of the GHP, towards 0.95 m. The phenomenon can be attributed to the condensed working fluid accumulating at 0.95 m, resulting in reduced heat release in other areas. Additionally, the return flow of highly condensed liquid reduces the temperature in other locations. The changes in temperature curves from Figure 8c–f provide further evidence to support this analysis.

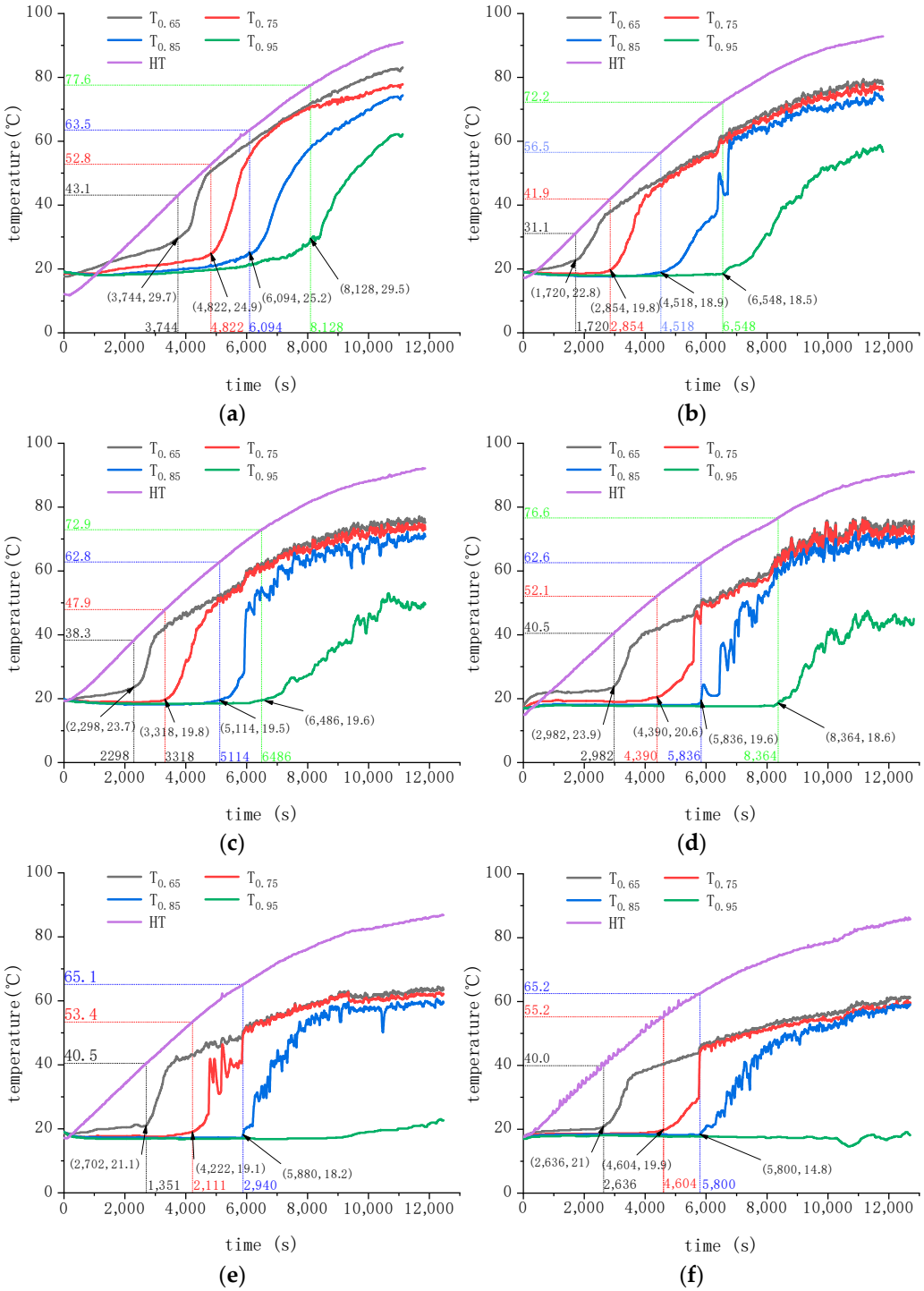

Figure 8. Influence of different wind speeds on the temperature of each point of GHP. (**a**) When the wind speed is 0 m/s, the temperature change curve of each temperature measuring point of the GHP. (**b**) When the wind speed is 0.3 m/s, the temperature change curve of each temperature measuring point of the GHP. (**c**) When the wind speed is 0.5 m/s, the temperature change curve of each temperature measuring point of the GHP. (**d**) When the wind speed is 1.0 m/s, the temperature change curve of each temperature measuring point of the GHP. (**e**) When the wind speed is 2.0 m/s, the temperature change curve of each temperature measuring point of the GHP. (**f**) When the wind speed is 2.5 m/s, the temperature change curve of each temperature measuring point of the GHP.

From the results shown in Figure 8c, it is evident that with an increase in wind speed from 0.3 m/s to 0.5 m/s, there is a slight rise in the start-up temperature at the four measuring points. The temperatures at 0.65 m, 0.75 m, 0.85 m, and 0.95 m are recorded as 38.3 °C, 47.9 °C, 62.8 °C, and 72.9 °C, respectively. These values show an increase of 23.2%, 14.3%, 11.2%, and 1.0%, respectively. The magnitude of the temperature increase is higher at lower positions and lower at higher positions. This phenomenon occurs because the working fluid needs to accumulate a certain amount of heat before the GHP can start, and the heat accumulates gradually, causing the working fluid to slowly vaporize. The wind facilitates the gradual vaporization of the working fluid within the GHP, thus aiding in the release of heat. Consequently, higher temperatures and longer accumulation periods are required for the heat pipe to initiate. In comparison to Figure 8b, the temperature fluctuations at each point are more apparent during the later stages of start-up, and the temperatures at 0.65 m, 0.75 m, and 0.85 m exhibit good isothermal characteristics.

Figure 8d demonstrates that with a further increase in wind speed from 0.5 m/s to 1.0 m/s, the start-up temperature of the four measuring points continues to increase, but with enhanced fluctuations. Notably, the isothermal characteristics at 0.65 m, 0.75 m, and 0.85 m also become more pronounced.

Figure 8e,f reveal that when the wind speed reaches 2.0 m/s, the GHP fails to start at 0.95 m, indicating that the working fluid hardly reaches this point for internal vaporization. In contrast to Figure 8b–d, the temperature fluctuations at 0.65 m, 0.75 m, and 0.85 m are significantly reduced. This indicates that when the wind speed surpasses this value, the heat carried away by the wind exceeds the heat transferred from the heating section to the GHP.

Based on the above analysis, an increase in wind speed makes the final stable temperature values at 0.65 m, 0.75 m, and 0.85 m converge closer to each other, while simultaneously decreasing their respective values. As the wind speed increases, the amplitude of the temperature fluctuations on the curves also increases. The start-up point at 0.95 m shifts left and then right with increasing wind speed. When the wind speed exceeds 2.0 m/s, the temperature at 0.95 m fails to reach the starting point. Moreover, as the wind speed increases, the GHP operates in an "unsaturated state", allowing for a higher maximum temperature limit. Hence, at a wind speed of 1.0 m/s, the GHP exhibits better start-up and isothermal characteristics.

3.5. Influence of Wind Speed on Thermoelectric Performance of GHP

The impact of wind speed on the thermoelectric generation behavior of the GHP is illustrated in Figure 9. The experimental conditions include a heating temperature range of 0 to 100 °C, an initial absolute pressure of 0.002 MPa, a heating height of 600 mm, and a working fluid height of 300 mm. The start-up characteristics and variations in thermoelectric generation of the GHP were investigated at different wind speeds: 0 m/s, 0.3 m/s, 0.5 m/s, 1.0 m/s, 2.0 m/s, and 2.5 m/s.

At a wind speed of 0 m/s, with a heating temperature of 71.2 °C, the voltage of the thermoelectric generator starts to rise, while the current has not yet initiated, as shown in Figure 9a. As the heating temperature increases to 82.8 °C, the current generated by the thermoelectric generator undergoes obvious changes.

When the wind speed is increased to 0.3 m/s, the start-up temperatures for both current and voltage noticeably decrease, as depicted in Figure 9b. The voltage of the thermoelectric generator begins to rise at a heating temperature of 66.4 °C, and the current initiates at 74.7 °C. The start-up temperature for voltage decreases by 6.74%, and the start-up temperature for current decreases by 9.78%. It can be observed from the figure that the final values of current and voltage generated by the thermoelectric generator chip have significantly improved.

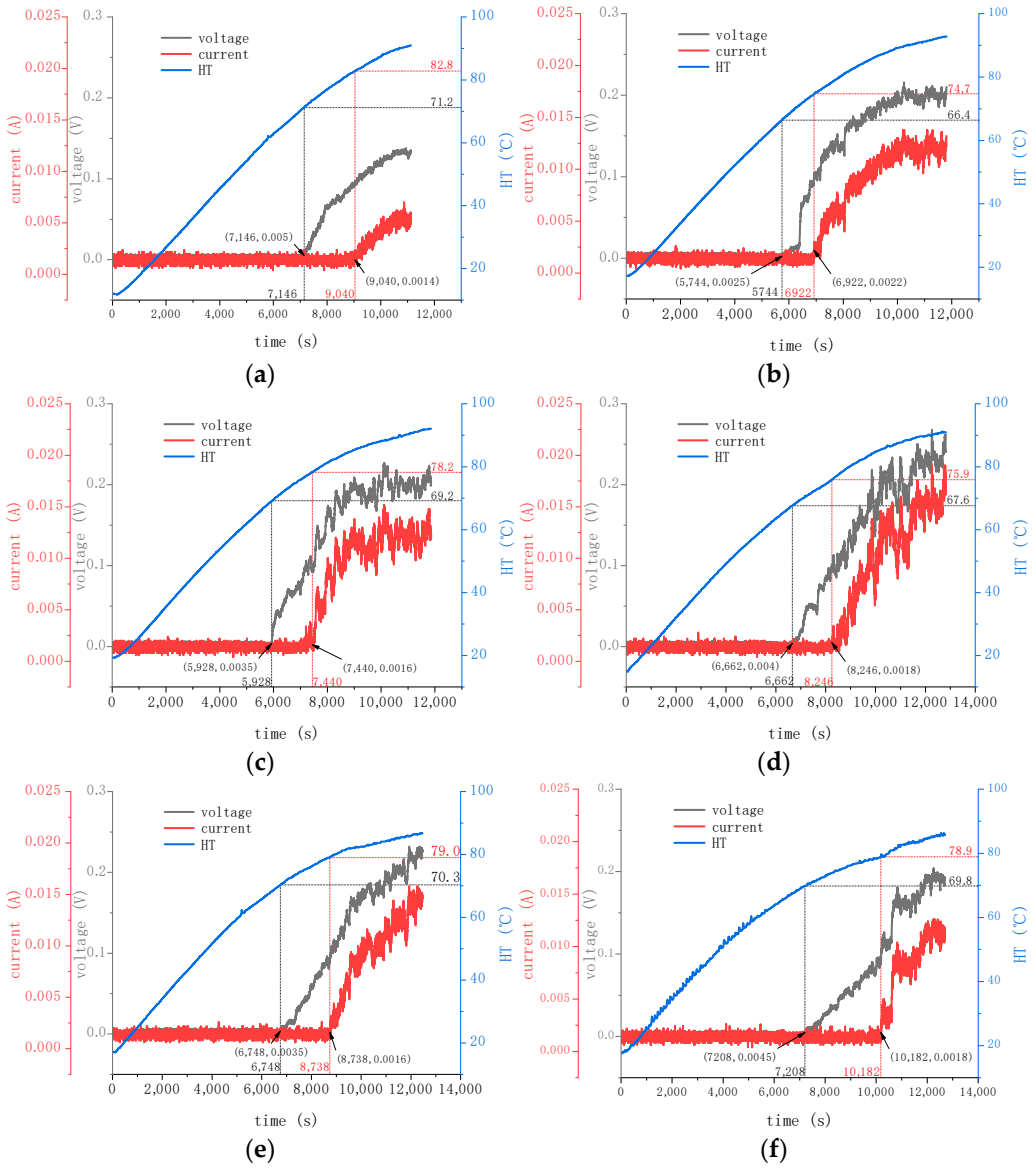

Figure 9. Influence curve of wind speed on thermal power generation by GHP. (**a**) When the wind speed is 0 m/s, the variation curve of thermoelectric generator of GHP. (**b**) When the wind speed is 0.3 m/s, the variation curve of thermoelectric generator of GHP. (**c**) When the wind speed is 0.5 m/s, the variation curve of thermoelectric generator of GHP. (**d**) When the wind speed is 1.0 m/s, the variation curve of thermoelectric generator of GHP. (**e**) When the wind speed is 2.0 m/s, the variation curve of thermoelectric generator of GHP. (**f**) When the wind speed is 2.5 m/s, the variation curve of thermoelectric generator of GHP.

When the wind speed is increased to 0.5 m/s, and the heating temperature reaches 69.2 °C, the voltage of the thermoelectric generator exhibits an upward trend. Similarly, at a heating temperature of 78.2 °C, the current of the thermoelectric generator starts to rise, as illustrated in Figure 9c. Compared with the previous case shown in Figure 9b, there is a slight increase in the start-up temperature for both current and voltage. The current increases by 4.22% and the voltage increases by 4.69%. Throughout the start-up process, noticeable fluctuations are observed in the current and voltage curves. The maximum stabilized values of current and voltage are almost consistent with the values observed in Figure 9b.

Upon further increasing the wind speed to 1.0 m/s, the voltage of the thermoelectric generator begins to rise at a heating temperature of 67.6 °C, while the current initiates at

75.9 °C, as depicted in Figure 9d. There is a slight decrease in the start-up temperature for both current and voltage compared to the curve shown in Figure 9c. Specifically, the voltage decreases by 1.41% and the current decreases by 2.94%. It can be observed that the current and voltage curves generated by the thermoelectric generator under a wind speed of 1.0 m/s exhibit significant fluctuations.

At a wind speed of 2.0 m/s, the voltage of the thermoelectric generator starts to rise when the heating temperature reaches 70.3 °C. Similarly, the current initiates at a heating temperature of 79.0 °C, as shown in Figure 9e. The start-up temperature for both current and voltage slightly increases compared to the curve at 1.0 m/s. Specifically, the voltage increases by 3.99% and the current increases by 4.08%. It can be observed that the fluctuation amplitude of the current and voltage curves generated by the thermoelectric generator decreases when the wind speed is 2.0 m/s.

Finally, when the wind speed reaches 2.5 m/s, the voltage of the thermoelectric generator starts to rise at a heating temperature of 69.8 °C, while the current initiates at a heating temperature of 78.9 °C, as shown in Figure 9f. The start-up temperature for both current and voltage slightly decreases compared to the curve depicted in Figure 9e. Specifically, the voltage drops by 0.71% and the current drops by 0.13%. It can be observed from the figure that the fluctuation amplitude of the current and voltage curves generated by the thermoelectric generator with a wind speed of 2.5 m/s is further reduced.

Figure 10 presents the average values and variances of current and voltage data generated by the thermoelectric generator during the stable stage under various wind speeds. It is evident from the results that the highest current and voltage values are obtained when the wind speed is 1.0 m/s. Additionally, the variance curve reveals that the fluctuation amplitude of the current curve is most pronounced at a wind speed of 1.0 m/s. Similarly, for a wind speed of 2.0 m/s, the variance of the voltage curve is the largest.

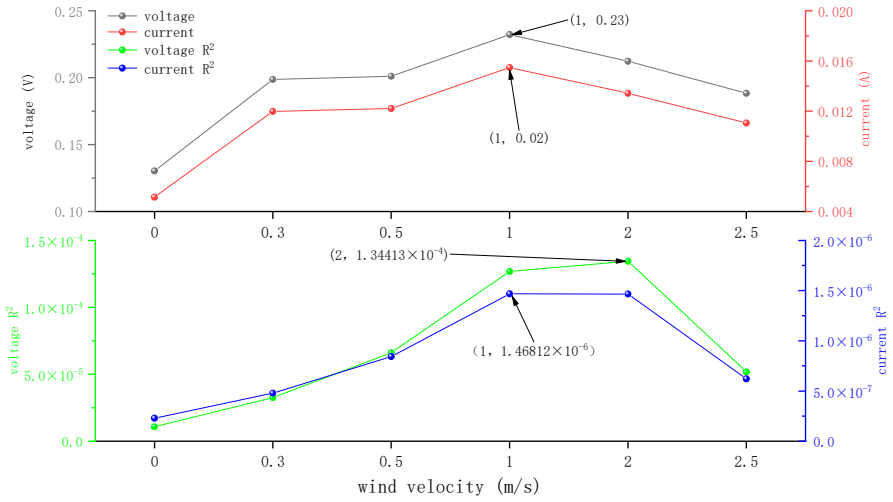

Figure 10. Mean value curve and variance curve of thermoelectric generation of GHP under different wind speeds.

This phenomenon can be attributed to the installation position of the thermoelectric generator at a height of 0.9 m. As the wind speed increases from 0 m/s, the circulation efficiency of the working fluid within the heat pipe improves, resulting in enhanced heat transfer at the location of the thermoelectric generator. Simultaneously, the increased wind speed accelerates heat dissipation on the opposite side of the thermoelectric generator, leading to a higher temperature difference. However, as the wind speed continues to rise, the airflow transitions from laminar flow to turbulent flow, causing uneven heat dissipation and resulting in greater variance in current and voltage.

When the wind speed exceeds or equals 2.0 m/s, the temperature at the 0.9 m position of the generator heat pipe begins to drop, leading to a reduction in temperature difference

and a consequent decline in power generation. Under these conditions, the temperature drop becomes the primary factor impacting performance, while the instability of the flow field is insufficient to further increase the variance of current and voltage. Consequently, the variance of current and voltage starts to decrease.

In summary, the optimal performance of thermoelectric generation occurs within the range of 1.0 to 2.0 m/s wind speeds. At these levels, the thermoelectric generator exhibits the highest power output.

4. Conclusions

This study explores the optimal parameters and optimal wind speed of GHPs for temperature difference power generation based on the deep-seated temperature accumulation in coal mine gangue dumps. Firstly, the optimal heating height and working fluid height of the GHP were studied, and then the influence of wind speed on temperature difference power generation was investigated. The following conclusions were drawn:

(1) Through the comparative experimental analysis of the heating height, when the heating height is 600 mm, the GHP shows good start-up characteristics and isothermal characteristics. Therefore, it can be judged that the heating height is 600 mm, and the performance of the GHP is optimal.

(2) When the heating height is 600 mm, the working fluid heights were adjusted to 200 mm, 300 mm, and 400 mm, respectively. Through comparative experiments, it was found that the variation of working fluid height has little effect on the final start-up temperature of GHP. When the working fluid height is 300 mm, the temperature curves of the four temperature measurement points fluctuate the least, and the start-up performance of the heat pipe is the most stable.

(3) When GHP is fully started, the adjusted wind speed gradually increases from 0m/s to 0.3 m/s, 0.5 m/s, 1.0 m/s, 2.0 m/s, and 2.5 m/s. With the increase of heating temperature, the temperature values of the four temperature measurement points gradually decrease. The power generated by the thermoelectric generator initially increases and then decreases. When the wind speed is 2.0 m/s, the power generated by the thermoelectric generator is the highest, indicating that GHP has the best thermoelectric power generation performance when the wind speed is 2.0 m/s.

(4) The influence of wind speed on the start-up performance of the heat pipe was studied through comparative experiments. Gradually increasing the wind speed can make the temperature curves at 0.65 m, 0.75 m, and 0.85 m of GHP closer. The results indicate that these three points have better isothermal characteristics. When the wind speed is greater than or equal to 2.0 m/s, the temperature at 0.95 m will not start. Therefore, GHP exhibits better start-up characteristics and isothermal characteristics at a wind speed of 1.0 m/s.

(5) The influence of wind speed on the start-up characteristics of the thermoelectric generator was studied through comparative experiments. With the increase of wind speed, the current, voltage oscillations, and power generation amplitude of the thermoelectric generator increase first and then decrease. When the wind speed is 1.0~2.0 m/s, the power generated by the thermoelectric generator is the largest, and the amplitude of the curve is also the largest.

The research results provide new optimization solutions for the deep-seated temperature control of coal mine gangue dumps and temperature difference power generation from waste heat, overcoming the previous blind parameters of GHP in treating gangue dumps. Due to the small area of the temperature difference power generation sheets used in this study, the power generation is relatively small. In practical applications, if more temperature difference power generation sheets are covered in the condensation section of GHP, a larger amount of electricity can be generated.

Author Contributions: Conceptualization, B.Z. and R.Z.; methodology, B.Z.; validation, S.F.; formal analysis, Y.Z.; investigation, Y.Z.; resources, S.Z.; data curation, S.Z.; writing—original draft preparation, B.Z.; writing—review and editing, B.Z. and S.F.; visualization, B.Z. and S.F.; supervision, B.Z. and S.F.; project administration, B.Z.; funding acquisition, B.Z. and R.Z. All authors have read and agreed to the published version of the manuscript.

Funding: This material is based upon work supported in part by the National Natural Science Foundation of China [grant numbers 42102222] and the Basic Research Program of Shanxi Province Youth Research Science Institute [grant numbers 202203021212219].

Acknowledgments: This manuscript was improved by comments from X.Z.

Conflicts of Interest: The authors declare no conflict of interest.

References

1. Wu, D.; Wang, Y.; Wang, M.; Wei, C.; Hu, G.; He, X.; Fu, W. Basic Characteristics of Coal Gangue in a Small-Scale Mining Site and Risk Assessment of Radioactive Elements for the Surrounding Soils. *Minerals* **2021**, *11*, 647. [CrossRef]
2. Zhang, D.; Yang, X.S.; Deng, J.; Wen, H.; Xiao, Y.; Jia, H. Research on coal spontaneous combustion period based on pure oxygen adiabatic oxidation experiment. *Fuel* **2021**, *288*, 119651. [CrossRef]
3. Hu, Z.Q.; Zhu, Q.; Xu, J.J.; Zhang, X. Effect of Bactericides on Control of Acidification Pollution and Spontaneous Combustion of Coal Gangue Dumps in China and Its Mechanism. *Sustainability* **2020**, *12*, 6697. [CrossRef]
4. Zhao, N.; Zhang, Y.B.; Zhao, X.H.; Niu, J.R.; Shi, H.; Yang, N.; Gao, T.; Guo, L.N. Internal Temperature Variation on Spontaneous Combustion of Coal Gangue Dumps under the Action of a Heat Pipe: Case Study on Yinying Coal Mine in China. *Sustainability* **2022**, *14*, 9807. [CrossRef]
5. Salomatov, V.V.; Kuznetsov, G.V.; Syrodoy, S.V. The comparative analysis of heat transfer efficiency in the conditions of formation of ash deposits in the boiler furnaces, with taking into account the crystallization of slag during combustion of coal and water-coal fuel. *J. Phys. Conf. Ser.* **2017**, *891*, 012240. [CrossRef]
6. Peng, H.; Jia, X.L. Experimental study on heat energy recovery and utilization of coal gangue hill based on gravity heat pipe. *Energy Rep.* **2022**, *8*, 220–229. [CrossRef]
7. Wang, L.; Yang, D.; Zhang, Y.X.; Li, W.Q.; Kang, Z.Q.; Zhao, Y.S. Research on the reaction mechanism and modification distance of oil shale during high-temperature water vapor pyrolysis. *Energy* **2022**, *261*, 15. [CrossRef]
8. Chaudhry, H.N.; Hughes, B. Climate responsive behaviour of heat pipe technology for enhanced passive airside cooling. *Appl. Energy* **2014**, *136*, 32–42. [CrossRef]
9. Li, Z.S. Design and preliminary experiments of a novel heat pipe using a spiral coil as capillary wick. *Int. J. Heat Mass Transf.* **2018**, *126*, 1240–1251. [CrossRef]
10. Tian, Z.X.; Zhang, J.R.; Wang, C.L.; Guo, K.L.; Liu, Y.; Zhang, D.L.; Tian, W.X.; Qiu, S.Z.; Su, G.H. Experimental evaluation on heat transfer limits of sodium heat pipe with screen mesh for nuclear reactor system. *Appl. Therm. Eng.* **2022**, *209*, 118296. [CrossRef]
11. Hu, M.K.; Zheng, R.C.; Pei, G.; Wang, Y.Y.; Li, J.; Ji, J. Experimental study of the effect of inclination angle on the thermal performance of heat pipe photovoltaic/thermal (PV/T) systems with wickless heat pipe and wire-meshed heat pipe. *Appl. Therm. Eng.* **2016**, *106*, 651–660. [CrossRef]
12. Akkus, Y.; Nguyen, C.T.; Celebi, A.T.; Beskok, A. A first look at the performance of nano-grooved heat pipes. *Int. J. Heat Mass Transf.* **2019**, *132*, 280–287. [CrossRef]
13. Zuo, Z.J.; North, M.T.; Wert, K.L. High heat flux heat pipe mechanism for cooling of electronics. *IEEE Trans. Compon. Packag. Technol.* **2001**, *24*, 220–225. [CrossRef]
14. Mahdavi, M.; Tiari, S.; De Schampheleire, S.; Qiu, S.G. Experimental study of the thermal characteristics of a heat pipe. *Exp. Therm. Fluid Sci.* **2018**, *93*, 292–304. [CrossRef]
15. Zhang, J.; Ren, Y.; Zhang, L.H.; Liang, H.M. Analysis of influencing factors of heat transfer performance of Heat pipe heat exchanger. In Proceedings of the 2019 International Conference on Energy and Environment Technology (ICEET 2009), Guilin, China, 16–18 October 2009; pp. 37–40. [CrossRef]
16. Xiong, Y.X.; Bo, L.; Qiang, M.; Wu, Y.T.; Zhang, X.X.; Xu, P.; Ma, C.F. A characteristic study on the start-up performance of molten-salt heat pipes: Experimental investigation. *Exp. Therm. Fluid Sci.* **2017**, *82*, 433–438. [CrossRef]
17. Jung, E.G.; Boo, J.H. Enhancement of the maximum heat transfer rate of the heat pipe through the bypass line. *Appl. Therm. Eng.* **2021**, *198*, 117461. [CrossRef]
18. Naruka, D.S.; Dwivedi, R.; Singh, P.K. Experimental inquisition of heat pipe: Performance evaluation for different fluids. *Exp. Heat Transf.* **2020**, *33*, 668–682. [CrossRef]
19. Jeyadevan, B.; Koganezawa, H.; Nakatsuka, K. Performance evaluation of citric ion-stabilized magnetic fluid heat pipe. *J. Magn. Magn. Mater.* **2005**, *289*, 253–256. [CrossRef]
20. Goshayeshi, H.R.; Goodarzi, M.; Safaei, M.R.; Dahari, M. Experimental study on the effect of inclination angle on heat transfer enhancement of a ferrofluid in a closed loop oscillating heat pipe under magnetic field. *Exp. Therm. Fluid Sci.* **2016**, *74*, 265–270. [CrossRef]

21. Shang, F.M.; Yang, Q.J.; Fan, S.L.; Liu, C.Y.; Liu, J.H. Experimental study on novel pulsating heat pipe radiator for horizontal cpu cooling under different wind speeds. *Therm. Sci.* **2022**, *26*, 449–462. [CrossRef]
22. Dang, C.; Jia, L.; Lu, Q.Y. Investigation on thermal design of a rack with the pulsating heat pipe for cooling CPUs. *Appl. Therm. Eng.* **2017**, *110*, 390–398. [CrossRef]
23. Yin, N.N.; Zhang, Z.; Wang, L.P.; Qian, K.M. Variations in organic carbon, aggregation, and enzyme activities of gangue-fly ash-reconstructed soils with sludge and arbuscular mycorrhizal fungi during 6-year reclamation. *Environ. Sci. Pollut. Res.* **2016**, *23*, 17840–17849. [CrossRef] [PubMed]
24. Kundan, A.; Plawsky, J.L.; Wayner, P.C., Jr.; Chao, D.F.; Sicker, R.J.; Motil, B.J.; Lorik, T.; Chestney, L.; Eustace, J.; Zoldak, J. Thermocapillary Phenomena and Performance Limitations of a Wickless Heat Pipe in Microgravity. *Phys. Rev. Lett.* **2015**, *114*, 146105. [CrossRef] [PubMed]
25. Huang, J.L.; Xiang, J.H.; Chu, X.Y.; Sun, W.J.; Liu, R.L.; Ling, W.S.; Zhou, W.; Tao, S.L. Thermal performance of flexible branch heat pipe. *Appl. Therm. Eng.* **2021**, *186*, 116532. [CrossRef]
26. Wang, H.G.; Bao, Y.H.; Liu, M.; Zhu, S.; Du, X.P.; Hou, Y. Experimental study on dynamic characteristics of cylindrical horizontal axially rotating heat pipe. *Appl. Therm. Eng.* **2022**, *209*, 118248. [CrossRef]
27. Zhang, X.; Jiang, D.Y.; Wang, H.; Liu, X.D. Experimental analysis on the evaporator startup behaviors in a trapezoidally grooved heat pipe. *Appl. Therm. Eng.* **2021**, *199*, 117558. [CrossRef]
28. Hashimoto, M.; Akizuki, Y.; Sato, K.; Ueno, A.; Nagano, H. Proposal, transient model, and experimental verification of loop heat pipe as heating device for electric-vehicle batteries. *Appl. Therm. Eng.* **2022**, *211*, 118432. [CrossRef]
29. Liu, C.P.; Chen, Y.; Feng, D.L.; Zhang, H.X.; Miao, J.Y.; Feng, Y.H.; Yan, Y.Y.; Zhang, X.X. Experimental study on temperature uniformity and heat transfer performance of nitrogen loop heat pipe with large area and multi-heat source. *Appl. Therm. Eng.* **2022**, *210*, 118344. [CrossRef]
30. Wu, Y.P.; Jia, J.; Tian, D.M.; Chuah, Y.K. Heat Transfer Performance of Microgroove Back Plate Heat Pipes with Working Fluid and Heating Power. *J. Therm. Sci.* **2020**, *29*, 982–991. [CrossRef]
31. Barba, M.; Bruce, R.; Bouchet, F.; Bonelli, A.; Baudouy, B. Effects of filling ratio of a long cryogenic Pulsating Heat Pipe. *Appl. Therm. Eng.* **2021**, *194*, 117072. [CrossRef]
32. Wu, G.Q.; Gou, X.; Li, B. Experimental Study on Heat Transfer Performance of Elliptical Loop Heat Pipe. In Proceedings of the 3rd IEEE International Electrical and Energy Conference (CIEEC), Beijing, China, 7–9 September 2019; pp. 1591–1596. [CrossRef]
33. Zhao, Y.L.; Fan, Y.C.; Li, W.J.; Li, Y.Z.; Ge, M.H.; Xie, L.Y. Experimental investigation of heat pipe thermoelectric generator. *Energy Conv. Manag.* **2022**, *252*, 115123. [CrossRef]